# Lab on a Chip

Accepted Manuscript

This is an *Accepted Manuscript*, which has been through the Royal Society of Chemistry peer review process and has been accepted for publication.

Accepted Manuscripts are published online shortly after acceptance, before technical editing, formatting and proof reading. Using this free service, authors can make their results available to the community, in citable form, before we publish the edited article. We will replace this *Accepted Manuscript* with the edited and formatted *Advance Article* as soon as it is available.

You can find more information about *Accepted Manuscripts* in the **Information for Authors**.

Please note that technical editing may introduce minor changes to the text and/or graphics, which may alter content. The journal's standard **Terms & Conditions** and the **Ethical guidelines** still apply. In no event shall the Royal Society of Chemistry be held responsible for any errors or omissions in this *Accepted Manuscript* or any consequences arising from the use of any information it contains.
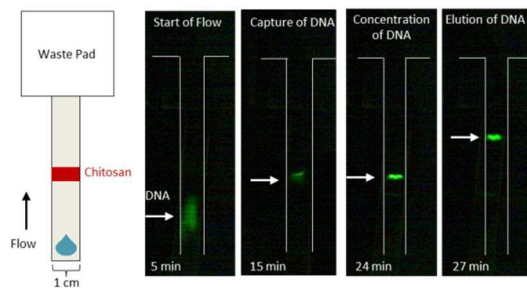
One-step purification and concentration of DNA in porous membranes for point-of-care applications

S. A. Byrnes, J.D. Bishop, L. Lafleur, J. R. Buser, B. Lutz, and P. Yager

Nucleic acid purification in porous membranes at the point-of-care from complex samples including nasal matrix and blood using a single-user step.

Lab on a Chip

ARTICLE

One-step purification and concentration of DNA in porous membranes for point-of-care applications

S. A. Byrnes*, J. D. Bishop, L. Lafleur, J. R. Buser, B. Lutz, and P. Yager

The emergence of rapid, user-friendly, point-of-care (POC) diagnostic systems is paving the way for better disease diagnosis and control. Lately, there has been a strong emphasis on developing molecular-based diagnostics due to their potential for greatly increased sensitivity and specificity. One of the most critical steps in developing practical diagnostic systems is the ability to perform sample preparation, especially the purification of nucleic acids (NA), at the POC. As such, we have developed a simple-to-use, inexpensive, and disposable sample preparation system for in-membrane purification and concentration of NAs. This system couples lateral flow in a porous membrane with chitosan, a linear polysaccharide that captures NAs via anion exchange chromatography. The system can also substantially concentrate the NAs. The combination of these capabilities can be used on a wide range of sample types, which are prepared for use in downstream processes, such as qPCR, without further purification.

Introduction

According to the WHO, the types of diagnostics used around the world have been shifting from traditional laboratory-based tests, such as ELISA and qPCR, to rapid test formats; the aim is to deliver diagnosis at the point-of-care (POC). From 1999 to 2009, the proportion of HIV rapid tests procured globally increased from ~35% to over 80%[1]. This trend reached a peak in 2007 with over 95% of procurements being of the rapid test variety[1]. Although this trend is encouraging, there is still a gap in the availability of accurate diagnostics for the POC.

According to the 2010 Global Burden of Disease study, four of the top ten causes of death world-wide are attributed to communicable diseases, which disproportionally affect low resource settings (LRS)[2–4]. Of these top ten, number four is lower respiratory infections and seven is diarrhea[2–4]. Each of these conditions can be caused by multiple pathogens; without a proper diagnosis, accurate treatment cannot be provided. In developed settings, these diagnoses are often performed through nucleic acid (NA) detection. The use of NA for disease diagnosis offers multiple advantages including increased sensitivity, the ability to multiplex, and epidemiological tracking of disease transmission and drift via NA sequencing. These approaches, however, are not available at the POC because they often rely on sample pre-treatment techniques that require expensive equipment and highly trained personnel.

Common methods of DNA purification used in both laboratory settings and tests designed for the POC often rely on one of three general mechanisms: solid-phase extraction, electrostatic interactions, or sequence-specific capture. One of the most widely used techniques is solid-phase extraction (SPE) with silica particles. Pioneering work by Boom *et al.* demonstrated a "rapid and simple" method for nucleic acid purification using chaotropic agents, ethanol, and an acidic silica slurry. Their method cited a total assay time of less than one hour for greater than 50% recovery of DNA[5]. The current gold standard Qiagen kit utilizes a similar technique with silica particles embedded in a centrifugal filter for NA isolation from complex samples. Other common laboratory techniques rely on NA precipitation in the presence of solutions with high alcohol content[6]. Although these traditional methods are well characterized and reliable, they often require expensive laboratory equipment and highly trained laboratory technicians, limiting their availability in the developed and developing world to centralized facilities and hospitals.

Over the last 20 years, the field of microfluidics has aimed to address and overcome the gap between laboratory capabilities and POC systems through the development of single-use, plastic microfluidic chips[7]. There have been numerous publications about the wide range of applications for these chips including cell lysis and NA purification[8,9], sample concentration[10], immunoassays[11–13], and NA amplification[14,15].

Gubala *et al.* extensively reviewed many of these pioneering applications[16].

In the microchip format, NA purification for the POC often adapts techniques from traditional laboratory methods. For example, multiple groups have published on the use of SPE membranes in microfluidic devices[17–20]. The Klapperich group embedded silica particles in a porous polymer monolith (PPM) within microfluidic channels to combine DNA purification from complex samples with on-chip PCR[21–23]. The Bau group designed a sample-to-answer polycarbonate cassette with on-chip reagent storage for NA isolation using a silica membrane[24]. There has also been initial work published on the use of sequence-specific capture for isolating NA targets in microfluidic chips[25,26].

Another widely used technique for DNA purification in microfluidic devices exploits the negative charge of DNA molecules; DNA can associate with coated magnetic beads[27,28], cationic polymers[29–31] or resins[32], and can be separated through electrophoretic methods[33–35]. The Landers group utilized chitosan, a cationic polymer, to selectively isolate NAs in a microchip from complex solutions[36–39]. Chitosan is a linear polymer comprised of linked sugar rings with a primary amine functional group on each monomer. Below its pK_a (6.3-6.5[40]) the amine is protonated, and the polymer becomes polycationic. At higher pH values, the amine is deprotonated and returns to an uncharged state. This charge reversal enables a controllable electrostatic attraction between NAs and chitosan at low pH values that can be reversed through a buffer exchange. Early work with the chitosan-NA interaction focused on NA compaction and delivery for gene therapy applications[41–43]. Although many of the above microchip-based systems show promise for translation to realistic POC systems, there is a drawback to their implementation due to the use of potentially expensive equipment for operation (e.g.: syringe pumps). Devices that require this type of equipment have limited usability in POC settings such as a patient's home or rural health clinics in the developing world. Due to these constraints, many groups have begun to focus on an alternative platform for diagnostics: porous membranes.

The use of porous membranes, or paper-based substrates, as a platform for bioassays dates back to the 1930s with the development of paper chromatography[44–46]. In the mid to late-1970s the home-based pregnancy test brought paper-based diagnostics to the POC[47–49]. More recently, George Whitesides' group began patterning cellulose paper to simultaneously detect glucose and proteins in urine samples[50]. The field has also evolved beyond one-dimensional lateral flow systems to include two-dimensional paper networks (2DPN)[51], which offer advantages such as the ability to perform complex, multi-step processes[52], the sequential timed delivery of reagents[51,53], and compatibility with various detection techniques[54]. Porous-membrane-based assays do not require mechanical pumps because capillarity wicks fluids into and through the paper[37]. These devices are also inexpensive, easy to manufacture, and disposable, making them ideal candidates for POC tests. Two recent reviews detail the use of porous

membrane-based microfluidics for diagnostic devices[55] and the translation of multi-step processes from laboratory gold-standard techniques to paper-based systems[56].

There is still a significant gap in translating NA tests to paper platforms, especially those that may require NA purification and concentration. Mariella *et al.* noted that few paper-based devices have developed reliable solutions for the use of NA in paper-based formats[57]. Recent publications have detailed systems that isolate NAs using commercially available extraction membranes such, as FTA or Fusion 5[58,59], or chromatography paper[60]. Although these membranes do selectively isolate NAs, they have only been demonstrated in conjunction with plastic microchips or require minimal equipment with multiple user steps.

Furthermore, sample concentration can be an additional critical step in the NA purification process, especially for environmental testing where only a few targets may be present in large volumes (mL to L) of sample. As such, an ideal porous membrane-based NA purification system should also substantially concentrate the target.

In this work, a novel DNA purification and concentration system that uses the linear polysaccharide chitosan was developed in porous membrane substrates for POC applications. It is well known that surfaces can be modified with polymers to engineer or control surface properties such as charge[61,62]; we've used these principles to investigate chitosan's interaction with two different porous membranes. Second, the capacity of different membranes for the polymer and polymer retention during lateral flow were measured. These steps provide a quantitative method for determining the capacity for DNA binding of chitosan-coated membranes. Finally, on the basis of this method, a system was developed and tested using porous membranes to simultaneous purify and concentrate DNA from complex samples containing high protein content, excess non-target DNA, and blood. Further, the purification system uses a novel, one-step, sequential reagent delivery mechanism developed in the Yager and Lutz labs[63,64] that directly translates to a simple, one-step user experience; this further supports the feasibility of this system for use in POC applications.

Materials and Methods

Reagent preparation

All reagents were prepared with sterile molecular biology grade water (Thermo Fisher Scientific, Waltham, MA). Low molecular weight chitosan oligosaccharide lactate (average MW 5000), mucin from porcine stomach Type III, sodium chloride, Tris-HCl, and MES were purchased from Sigma Aldrich (St. Louis, MO). Pulse-field-certified agarose, sample loading dye, SYBR Gold gel stain, and DNA ladders were purchased from BioRad (Hercules, CA). A 10x stock of TBE buffer was purchased from Thermo Fisher Scientific (Waltham, MA). Human genomic DNA (gDNA) was purchased from Promega (Madison, WI). The 50 mM MES DNA capture and

wash buffers were prepared in sterile water and the pH was adjusted to 5. The 50 mM Tris DNA elution buffer was prepared in sterile water with red food coloring (Safeway, Pleasanton, CA) to track fluid flow; the pH was adjusted to 9. The simulated nasal matrix (SNM) was prepared as previously described[65]. Defibrinated sheep's blood was purchased from Hemostat Laboratories (Dixon, CA).

Device patterning and construction

All porous membranes and test card materials were cut using a CO_2 laser (Universal Laser Systems, Scottsdale, AZ). Untreated, backed, 5-10 µm pore diameter nitrocellulose (NC) membranes (FF80HP, GE Healthcare Life Sciences, Niskayuna, NY) and untreated, unbacked, 10-100 µm pore diameter glass fiber (GF) membranes (Standard 17, GE Healthcare Life Sciences, Niskayuna, NY) were patterned with chitosan. Test cards were made with 0.254 mm-thick Mylar backing with adhesive (10 mil AC Melinex, Fralock, Valencia, CA) and cellulose wicking pads (CFSP223000 Millipore, Millipore, Billerica, MA) for waste fluid uptake.

The nitrocellulose and glass fiber membranes were patterned with a low molecular weight chitosan solution prepared in 50 mM MES at pH 5 using a piezoelectric noncontact printer (SciFLEXARRAYER S3, Scienion AG, Berlin, Germany). After printing, the membranes were stored in a desiccator. Membranes patterned with fluorescently tagged chitosan were also wrapped in foil to protect them from light and photobleaching.

SEM of porous membranes

All images were collected using an FEI Sirion electron microscope and samples were Au/Pd sputter coated (SPI Module Control, Structure Probe, Inc., West Chester, PA, USA) with an estimated 12 nm Au/Pd. A 5 kV beam was used for imaging (Fig. S1). Using these images, membrane surface area was estimated by representing the features as spheres and cylinders to simplify calculations. The calculated surface areas per volume of nitrocellulose and glass fiber were 2.0 $\mu m^2/\mu m^3$ and 0.19 $\mu m^2/\mu m^3$, respectively. These calculated values are consistent within an order of magnitude with other published values[66,67].

Fluorescent labeling of chitosan

Chitosan was fluorescently labeled using the commercially available 488 or 594 Amine-Reactive Dye Kit from Thermo Scientific (Logan, UT). Chitosan was dissolved in 50 mM MES at pH 5 to make a 1% w/v solution. After a one-hour incubation at room temperature with the amine-reactive dye, the chitosan was purified by precipitation using 5 M NaOH followed by centrifugation at 9400g for 3 minutes. The precipitated chitosan was re-dissolved in 50 mM MES and the pH was adjusted to 5 to prepare it for reagent patterning. The solution was stored in the dark at 4 °C for up to one month.

Purifying and fluorescent labeling of DNA

All DNA was purified from freshly cultured methicillin-sensitive *Staphylococcus aureus* (MSSA, strain RN4220) bacterial cells. The DNA was purified using the commercially available Qiagen Gentra Puregene Kit (Qiagen, Valencia, CA) with a slightly modified protocol. During the lysis step, 50 µL of lysostaphin (100 µg/mL) was added with the recommended 1.5 µL of Lytic Enzyme Solution provided by the kit. Purified DNA was resuspended in 20 µL of sterile water and incubated for 20 minutes at 65 °C to complete resuspension. The final DNA concentration was calculated by qPCR (described below).

After purification, DNA was fluorescently labeled using the Alexa Fluor 488 or 594 ARES DNA Labeling Kit (Life Technologies, Carlsbad, CA) with a slightly modified protocol. During the initial nick translation step, the concentration of each of the dNTPs was 0.5 mM. After labeling, the final concentration of the fluorescent DNA was determined using qPCR for the *ldh*-1 gene.

Pulse field gel electrophoresis for DNA fragment size

Pulse field gel electrophoresis (PFGE, Fig. S2) was used to determine the fragment size of DNA both before and after purification with chitosan in-membrane. A 1.0% agarose gel was prepared in 0.5x TBE buffer and set overnight at 4 °C. Gels were run using the BioRad CHEF Mapper XA System (BioRad, Hercules, CA) in a cold room (4 °C) in 0.5x TBE running buffer. Agarose plugs containing the high molecular weight *S. cerevisiae* DNA ladder were loaded into the gel before submerging in running buffer. Liquid samples were added to the gel with sample loading buffer. The "Auto-Algorithm" function was used with an input size range of 100 kbp to 2200 kbp. Gels were stained with 2x SYBR Gold in running buffer (limit of detection ~10^8 copies) for 20 minutes with shaking followed by 10 minutes of de-staining in DI water. Gels were imaged with the BioRad Gel Doc EZ System (BioRad, Hercules, CA).

qPCR for MSSA ldh-1 gene

DNA recovery was quantified with a qPCR kit for the *ldh*-1 gene provided by the ELITechGroup (ELITechGroup Molecular Diagnostics, Bothell, WA). The 20 µL reactions were run on a Rotorgene real-time PCR instrument (Qiagen, Valencia, CA) using the following protocol: 50°C hold for 2 minutes, 93°C hold for 2 minutes, 45 cycles of 93°C for 10 seconds, 56°C for 30 seconds, and 72°C for 15 seconds, ending with final elongation step at 72°C for 5 minutes. Fluorescence data were collected during the 56°C annealing step in the orange channel. The qPCR results were analyzed using the automated threshold cycle (CT) value calculation in the Rotorgene software (Qiagen, Valencia, CA). This assay is sensitive down to ~10^1 copies of the target sequence. The red dye or up to 0.5% blood in the elution buffer do not significantly interfere with the qPCR signal (Fig. S3).

Chitosan interactions with porous membranes

Porous membrane capacity for chitosan

To determine the capacity of each membrane for chitosan, small punches (radius = 2.4 mm) were taken from sheets of nitrocellulose and glass fiber. These punches were filled to capacity for nitrocellulose and glass fiber, 1.81 or 7.56 µL, respectively, with varying concentrations of fluorescent chitosan in solution to produce different chitosan concentrations in the membranes. Here, chitosan concentration is defined as µg of chitosan per μm^2 of membrane surface area ($\mu g/\mu m^2$), assuming even coating on all surfaces. The membranes were placed in clear Petri dishes and incubated in a dark chamber at 95% relative humidity for 24 hours to allow equilibration of chitosan adsorption to the membrane.

After incubation, the membranes were imaged wet to determine a baseline fluorescence signal for the input amount of chitosan. Next, the membranes were washed with 1x volume capacity of 50 mM MES at pH 5 and fluid was wicked away via a cellulose waste pad to remove unadsorbed chitosan. The membranes were re-wet with 50 mM MES at pH 5 and imaged a second time to track the loss in fluorescent signal. The loss of chitosan was measured as the difference between the baseline fluorescence and the post-wash fluorescence of the coated membranes. All fluorescence images were captured using an Axiovert fluorescence microscope (Zeiss, Thornwood, NY) fitted with a Retiga 1300i digital CCD camera (Quantitative Imaging Corporation, Surrey, BC, Canada). Images were taken with MicroManager software[68] using a 50 ms exposure and 2.5x objective.

Chitosan adsorption was calculated as the percent change in the integrated fluorescence intensity over the entire patterned region from pre- to post-wash conditions (**1**). These intensity values were measured using ImageJ[69].

$$\% \, adsorbed = \frac{fluorescence_{post-wash}}{fluorescence_{pre-wash}} \, x \, 100\% \qquad (1)$$

For both membranes, the chitosan concentrations tested ranged from 0 to 3.6×10^{-8} $\mu g/\mu m^2$. The upper limit of chitosan concentration for each membrane was bounded by the solubility of chitosan in buffer (50 mM MES, pH 5), the volume capacity, and the pore surface area of the membrane. Membrane capacity was determined by plotting the percent of chitosan adsorbed to each surface against the input chitosan concentration (in $\mu g/\mu m^2$) (Fig. S4C). These capacities were further verified by theoretical calculations based on the length of the chitosan polymer and the membrane surface areas; see the *Supplementary Information* (Fig. S4A and Fig. S4B) for the full calculations.

Chitosan retention in porous membranes during flow

To determine the retention of chitosan in each porous membrane during flow, a 2.5 mm long by 10 mm wide region of each membrane was patterned with fluorescent chitosan. Three concentrations were tested to determine if retention during flow was concentration dependent. The three tested concentrations for both membranes were based on the results of the previous adsorption studies. The concentrations in the patterned regions were 4.5×10^{-10}, 8.9×10^{-10}, and 1.3×10^{-9} $\mu g/\mu m^2$ for nitrocellulose and 8.9×10^{-10}, 1.8×10^{-9}, and 2.7×10^{-9} $\mu g/\mu m^2$ for glass fiber.

The patterned membranes were attached to 10 mil thick Mylar backing with adhesive (10 mil AC Melinex, Fralock, Valencia, CA) for ease of handling. An untreated cellulose pad (CFSP223000 Millipore, Billerica, MA), cut using the CO_2 laser cutter, was used as a waste collection reservoir. Before the initiation of flow, the chitosan regions on each membrane were wetted with 50 mM MES at pH 5 and excess unadsorbed chitosan were removed *via* wicking with a cellulose waste pad through the thickness of the membrane. This step was important to decouple the loss of chitosan due to incomplete adsorption to the membrane from the loss of chitosan during lateral flow.

To test chitosan retention during flow, two solutions were sequentially wicked through the membrane. These solutions were the DNA capture and elution buffers, which were selected to mimic an actual DNA purification experiment. The volume of the solutions was set to 2x the fluid capacity of the membrane (120 µL total for nitrocellulose and 500 µL total for glass fiber).

Dimensions of the patterned region and the fluorescence intensity of the chitosan were measured in ImageJ from uncompressed, time-lapse videos acquired using HandyAVI (AZcendant, Tempe, AZ, USA) in a humidified, light-tight box illuminated with two blue LEDs. Videos were captured using a web camera (Logitech, Fremont, CA) fitted with a 550 nm high-pass filter (FEL0550, Thor labs, Newton, NJ). The fluorescence intensity of the chitosan during flow was normalized to the initial wetted intensity to determine the percent of polymer retained in the membrane during flow.

DNA purification and concentration in porous membranes using chitosan

Chitosan is a linear polysaccharide with a primary amine functional group on every monomer. In solutions buffered below the polymer's pK_a, 6.3-6.5[40], the primary amine is protonated, resulting in a multivalent cationic polymer. In its protonated form, chitosan binds DNA and RNA *via* electrostatic interactions. When exposed to a solution above the pK_a, the primary amines are deprotonated and this electrostatic attraction is lost, resulting in release of nucleic acids (**Fig. 1**).
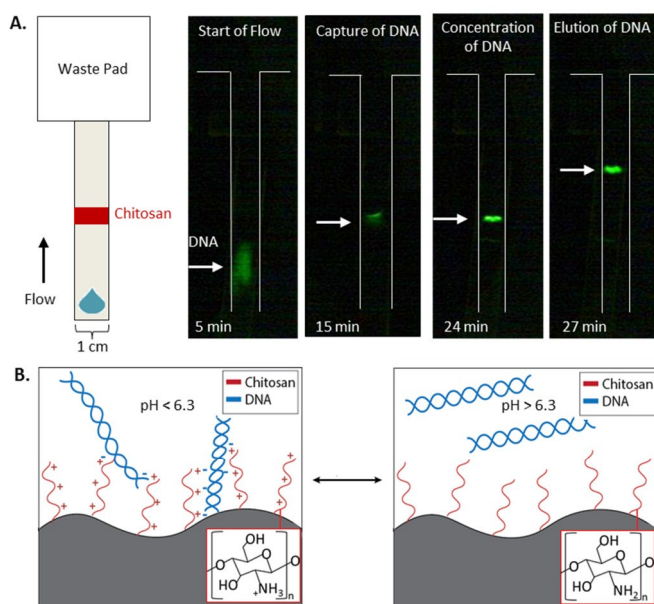
Fig. 1 DNA purification in porous membranes using chitosan. A) Schematic and images from a purification experiment in nitrocellulose. The DNA (green) is initially seen as a smear. As it reaches the chitosan region, DNA stops flowing and becomes concentrated. Once DNA is eluted, it remains concentrated. B) Schematic of a membrane surface patterned with chitosan (red). In solutions with a pH below 6.3, the primary amines on each monomer become protonated and can bind DNA. When the pH is increased above the amine pK_a, the charge on the polymer returns to neutral and DNA is released. Note that the quantum efficiency of the label changes with pH and immobilization.

To evaluate the ability of chitosan to purify and concentrate DNA in paper, 60 x 10 mm membranes were patterned with chitosan in 50 mM MES at pH 5. The patterned region was set to an area 2.5 mm long by 10 mm wide to remain consistent with the chitosan retention experiments. Based on the capacity and retention experiments, the chitosan concentrations in nitrocellulose and glass fiber were set to 1.3×10^{-9} and 1.8×10^{-9} $\mu g/\mu m^2$ ($\pm 5\%$), respectively.

Chitosan capacity for DNA and DNA concentration factor
Chitosan's capacity for DNA in both nitrocellulose and glass fiber was determined by increasing the concentration of DNA in the input sample until a decrease in the relative amount of DNA recovered was observed by qPCR. The range of input DNA concentrations tested in both membranes was between 1×10^5 copies (0.3 ng) to 4×10^8 copies (1200 ng) of fragmented MSSA DNA purified from cells. On average, the target DNA was less than 250-300 kbp long; larger DNA fragments are unable to flow through the pores of the membranes (Fig. S2).

For these experiments, DNA was spiked into 100 µL of DNA capture buffer. This solution was wicked into the membrane, followed sequentially by 100 µL of wash and

elution buffers for NC, and 250 µL of wash and elution buffers for GF to accommodate for the higher fluid capacity. These experiments were run in a humidified chamber to reduce effects from evaporation.

DNA was recovered post-elution by placing the membrane in a centrifugal filter tube (0.45 µm Nylon centrifugal filters, VWR, Radnor, PA) and centrifuging for 3 minutes at 10,000g (Fig. S6). These elution volumes were measured and the target DNA concentration was determined by qPCR.

Concentration effects were measured by adding 1×10^5 to 1×10^6 copies (0.3 to 3 ng) of DNA into 100, 200, 500, 1000, or 2000 µL of capture buffer. These solutions were wicked through a membrane patterned with chitosan followed sequentially by either 100 µL for NC or 250 µL for GF of DNA wash and elution buffers. Post-elution, the DNA purification efficiency (% recovery) was quantified by qPCR. The concentration factor was calculated as the initial input volume divided by the measured elution volumes times the % recovery (**2**).

$$Concentration\ Factor = \frac{Input\ volume}{Elution\ volume} \ x\ 100\% \qquad (2)$$

Recovery of DNA from complex samples
To determine the ability of a porous membrane pre-loaded with chitosan to purify DNA, approximately 1×10^5 to 1×10^6 copies of MSSA DNA was diluted into 100 µL of DNA capture buffer. The sample was wicked into the patterned membrane followed by wash and elution buffers, as described above. In addition to purification of DNA in water, the experiment was repeated with 1 µg BSA, 0.1% w/v mucins, 1% w/v mucins, up to 1000x non-target human gDNA, and 1% or 10% SNM to mimic more complex solutions. The percent recovery for each sample was determined by qPCR. These experiments were run in a humidified chamber to reduce effects of evaporation.

DNA purification from blood samples
Nucleic acid purification using chitosan patterned in porous membranes was also used to purify and concentrate DNA from blood samples. Often, blood preparation procedures require multiple user steps and removal of blood components that can inhibit downstream amplification reactions, notably heme[70]. From 15 to 50 µL of defibrinated sheep's blood was spiked into sample volumes ranging from 100 µL to 2000 µL. These samples were wicked into porous membranes patterned with chitosan followed by sequential delivery of wash and elution buffers, as described above. The purified DNA was analyzed by qPCR. These experiments were run in a humidified chamber to reduce effects of evaporation.

Statistics

All statistics were run using the open-source statistical package R (64 bit, version 3.0.2)[71].

Results and Discussion

Chitosan interaction with porous membranes

Porous membrane capacity for chitosan
In this work, we aimed to demonstrate a simple, porous membrane-based device that purifies and concentrates DNA from complex samples. We started with determining the amount of chitosan available to bind DNA when patterned onto different porous membranes. The amount of *available* chitosan should depend on its adsorption to the porous membrane.

For all concentrations tested in nitrocellulose, the amount of input chitosan that adsorbed to the membrane was above 90%, indicating that the membrane was not fully saturated with polymer. This same trend was not observed for glass fiber; at concentrations at or below $3.6x10^{-9}$ µg/µm^2, the percent of input chitosan adsorbed remained high. At concentrations above $3.6x10^{-9}$ µg/µm^2, the percent adsorbed dropped, indicating that the membrane capacity had been reached (Fig. S4C). These results are consistent with our understanding of the physical properties of these porous membranes; the high surface area of the nitrocellulose, with its small pores and features, provides a higher capacity (experimentally determined capacity: $3.3x10^{-8}$ µg/µm^2) for polymer adsorption than the coarser glass fiber (experimentally determined capacity: $\sim 5.4x10^{-9}$ µg/µm^2). This difference between nitrocellulose and glass fiber may be due to the way chitosan adsorbs to different surfaces. This data suggests that only a few monomers of the chitosan chain adsorb to nitrocellulose allowing more space for

additional molecules to adsorb. In glass fiber, on the other hand, a larger fraction of the total polymer might bind to the surface restricting the space available for other molecules to bind (Fig. S4A).

These empirical capacities were further supported by theoretical calculations that predict the chitosan capacity of nitrocellulose should be between $9.7x10^{-10}$ and $3.3x10^{-8}$ µg/µm^2. An adsorption capacity was not observed for the concentrations tested, up to $\sim 3.3x10^{-8}$ µg/µm^2, which is at the maximum of the theoretical range. Based on the theoretical calculations and empirically determined capacities, the chitosan coverage of the nitrocellulose surface was $\sim 100\%$ of the theoretical geometric monolayer coverage (Fig. S4B). For glass fiber, the theoretical capacity for chitosan should be between $9.5x10^{-10}$ and $3.2x10^{-8}$ µg/µm^2. The experimentally measured capacity for glass fiber falls within the lower range of the theoretical values and approximates to $\sim 15\%$ of the theoretical geometric monolayer coverage (Fig. S4B). Using these conditions, there is a monolayer of chitosan coverage on the nitrocellulose surface and less than a monolayer on glass fiber surface. The upper limit of chitosan concentration tested for each membrane was bounded by the solubility of chitosan in buffer (50 mM MES, pH 5) and the volume capacity of the membrane.

Chitosan retention in porous membranes during flow
The total amount of chitosan available for DNA binding (**Table 1**) is determined by the amount patterned onto the membrane minus losses from incomplete adsorption, described above, and capillary flow, described below.

Table 1. Final chitosan concentration in each membrane after accounting for losses from incomplete adsorption and flow. *The "mean final concentration" is based on the average percent adsorbed and retained. **The "Range final concentration" is based on the standard deviations for the percent retained during flow.

Input Concentration (µg/µm^2)	% adsorbed	% retained	Mean final concentration* (µg/µm^2)	Range final concentration** (µg/µm^2)
Nitrocellulose				
$4.5 x10^{-10}$	89 %	83 %	$3.3x10^{-10}$	$3.3x10^{-10} - 3.4x10^{-10}$
$8.9x10^{-10}$	85 %	74 %	$5.6x10^{-10}$	$5.4x10^{-10} - 5.7x10^{-10}$
$1.3x10^{-9}$	91 %	71 %	$8.6x10^{-10}$	$8.3x10^{-10} - 9.0x10^{-10}$
Glass Fiber				
$8.9x10^{-10}$	79 %	89 %	$6.3x10^{-10}$	$5.4x10^{-10} - 7.1x10^{-10}$
$1.8x10^{-9}$	58 %	71 %	$7.3x10^{-10}$	$6.8x10^{-10} - 7.8x10^{-10}$
$2.7x10^{-9}$	40 %	82 %	$8.7x10^{-10}$	$8.1x10^{-10} - 9.4x10^{-10}$

After characterizing the membrane capacity for chitosan, the effects of capillary flow on chitosan retention were measured. The three tested concentrations for nitrocellulose were $4.5x10^{-10}$, $8.9x10^{-10}$, and $1.3x10^{-9}$ µg/µm^2 and for glass fiber were $8.9x10^{-10}$, $1.8x10^{-9}$, and $2.7x10^{-9}$ µg/µm^2. The concentrations vary in nitrocellulose and glass fiber due to the different surface areas of each membrane. These values were based on high, medium, and low concentrations from the adsorption studies detailed above. Retention of chitosan in nitrocellulose is slightly concentration-dependent, with larger concentrations of patterned chitosan losing a higher percentage during flow (**Fig. 2A**). For glass fiber, this trend is not observed. The loss of chitosan due to flow does not appear to be concentration-dependent (**Fig. 2B**).

DNA purification and concentration in porous membranes using chitosan

Chitosan capacity for DNA and DNA concentration factor
Chitosan capacity for DNA in nitrocellulose and glass fiber was evaluated after optimizing adsorption and retention. The capacity for DNA in nitrocellulose was $1.9x10^6$ copies of DNA/µg of chitosan (c/µg) (95% CI: $2.9x10^5$ to $3.5x10^6$ c/µg). The capacity for DNA in glass fiber was $9.9x10^6$ c/µg (95% CI: $5.9x10^6$ to $1.4x10^7$ c/µg) (**Fig. 3**). These results are calculated using the mean final chitosan concentration from Table 1, which accounts for losses due to incomplete adsorption and retention. These data show that chitosan has a higher capacity for DNA in glass fiber than in nitrocellulose.
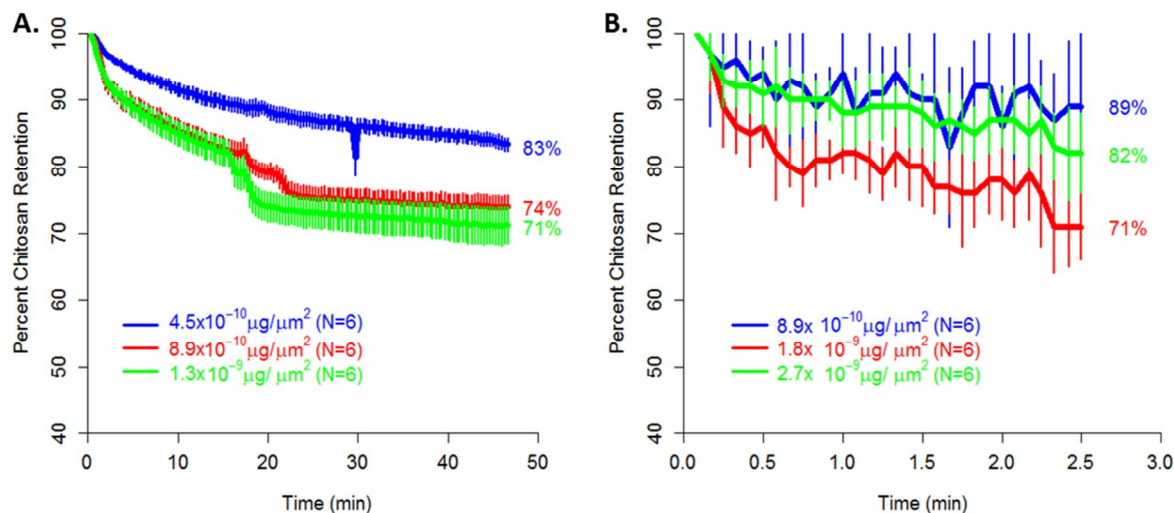
Fig. 2 Chitosan retention during flow after accounting for losses due to incomplete chitosan adsorption.   A) In nitrocellulose, retention during flow appears to be slightly concentration dependent. B) In glass fiber all three tested concentrations resulted in similar losses due to flow. The average retention (N=6) with +/- one standard deviation is plotted for each time point.

The smaller pores (10 µm) and higher surface area per volume (2.0 $\mu m^2/\mu m^3$) of nitrocellulose adsorbs more chitosan than glass fiber; but these results indicate that only a proportion of the chitosan is available for DNA binding in nitrocellulose. The chitosan used in this study was small, ~5000 MW. This size may allow polymer to integrate into the smallest pore features of nitrocellulose, some of which may be inaccessible to large DNA fragments (100s kbp), causing a high membrane capacity for the chitosan and a lower than expected binding capacity for DNA. Further, chitosan may hinder convective transport in the smaller pore features (or block flow completely) in nitrocellulose, reducing or preventing flow of DNA-containing sample through these membrane regions. On average, the pore features in glass fiber are larger (10-100 µm) and the material has a lower surface area per unit volume (0.19 $\mu m^2/\mu m^3$) than nitrocellulose (2.0 $\mu m^2/\mu m^3$). This reduced surface area lowers the overall chitosan capacity of the membrane, but may allow more of the chitosan to be available for DNA binding.

Using these results, the calculated ratio of positive (chitosan) to negative (DNA) charges when the system has reached its maximum capacity for DNA indicates that there is less than a monolayer of nucleic acid bound to the chitosan in both nitrocellulose and glass fiber (Fig. S5). These calculations assume that a full monolayer of DNA would equate to an equal ratio of charges at the DNA-chitosan binding capacity; see the *Supplementary Information* for the full calculations. Further, these estimates and calculations assume all of the chitosan patterned in the membrane, after accounting for losses presented in Table 1, is available for DNA binding. More reasonably, only some percentage would be available because some of the polymer is interacting with the membrane surface,

potentially rendering it unavailable for DNA binding. Additionally, both of these membranes have a range of pore size features and some fraction of the polymer may be trapped in the smallest of these features preventing it from interacting with DNA.   Both of these scenarios further support the calculations that there is less than a monolayer of nucleic acid bound to the chitosan in each membrane.
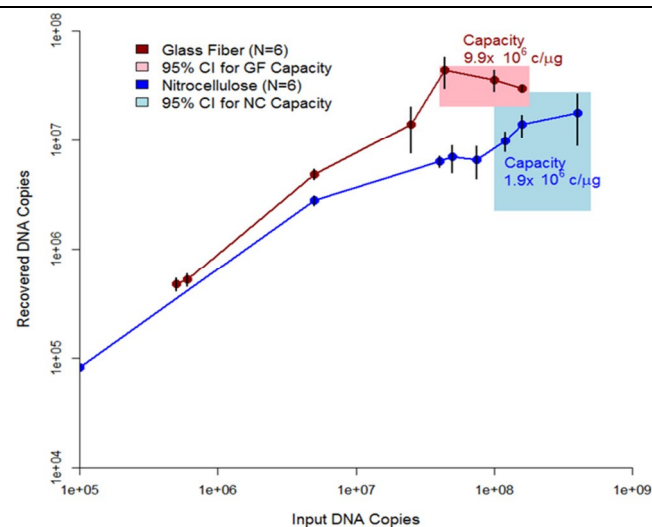
Fig. 3 Capacity of chitosan for DNA in nitrocellulose (blue) and glass fiber (red) over a range of input concentrations (N=6 for each point) after normalization for membrane surface area. The capacity of chitosan for DNA is 1.9×10^6 c/µg (95% CI: 2.9×10^5 to 3.5×10^6 c/µg) in nitrocellulose and 9.9×10^6 c/µg (95% CI: 5.9×10^6 to 1.4×10^7 c/µg) in glass fiber.

To enable broader use of these methods, the DNA capacities of each membrane have been converted to other common units (**Table 2**). Using the membrane capacity for chitosan and the chitosan capacity for DNA, this method can be adapted to capture and concentrate DNA from a variety of samples based on the expected amount of total nucleic acids.

Table 2. Chitosan capacity in nitrocellulose and glass fiber.
*Assuming average DNA fragment size of 2.0×10^5 bp.
**E. coli O157:H7, genome length 5.4×10^6 bp.
***MSSA RN4220, genome length 2.8×10^6 bp.

Capacity per µg chitosan	Nitrocellulose	Glass Fiber
copies DNA*	1.9×10^6	9.9×10^6
# bp*	3.8×10^{11}	2.0×10^{12}
ng DNA*	0.4	2.2
# *E. coli* bacteria**	7.0×10^4	3.7×10^5
# *MSSA* bacteria***	1.4×10^5	7.1×10^5

The maximum DNA concentration factors achieved with chitosan in nitrocellulose and glass fiber were 13.3x and 12.3x, respectively (**Fig. 4B**). These results are based on the input sample volume and the purification efficiency of DNA since each membrane type yielded a specific elution volume.

In nitrocellulose, which has a relatively homogenous pore size distribution, the interface between two sequentially delivered fluids is sharply defined. In this system, the wash and elution buffers have low and high pH values, respectively; the well-defined interface between the buffers under flow in nitrocellulose produces a sharp pH change (Fig. S6A). When the interface reaches the chitosan patterned region, the rapid change from low to high pH deprotonates the chitosan quickly, and releases purified DNA in a concentrated plug (Fig. S6B). In glass fiber, however, which has a relatively broad pore size distribution, the interface is poorly defined, which increases mixing between the two sequentially delivered buffers and causes a more gradual pH gradient to develop. When this gradient reaches the chitosan region, the gradual change from low to high pH deprotonates the chitosan slowly, resulting in a slower release (and therefore less concentrated plug) of purified DNA (Fig. S6C). In nitrocellulose, DNA samples always eluted in 8 µL while for glass fiber, the elution volume was 100-150 µL.

In this system, which involves complex surfaces in porous membranes as well as in-flow binding, both concentration factor and percent recovery were independent of the starting DNA concentration in the sample within the ranges tested. Using the data presented in Figure 3, the corresponding elution volumes, and the resulting recovery percentages (data not reported here), we measured consistent concentration factors and percent recovery for input DNA concentrations ranging from 1×10^3 copies of target per µL (c/µL) through 1×10^5 c/µL where total input volume was set to 100 µL. These concentrations were below the saturation limit of the modified membranes' binding capacity for DNA (measured in Fig. 3 and presented in Table 2). We have begun testing more dilute samples in larger input volumes and have preliminary data indicating this trend holds. That data will be the included in a future publication.
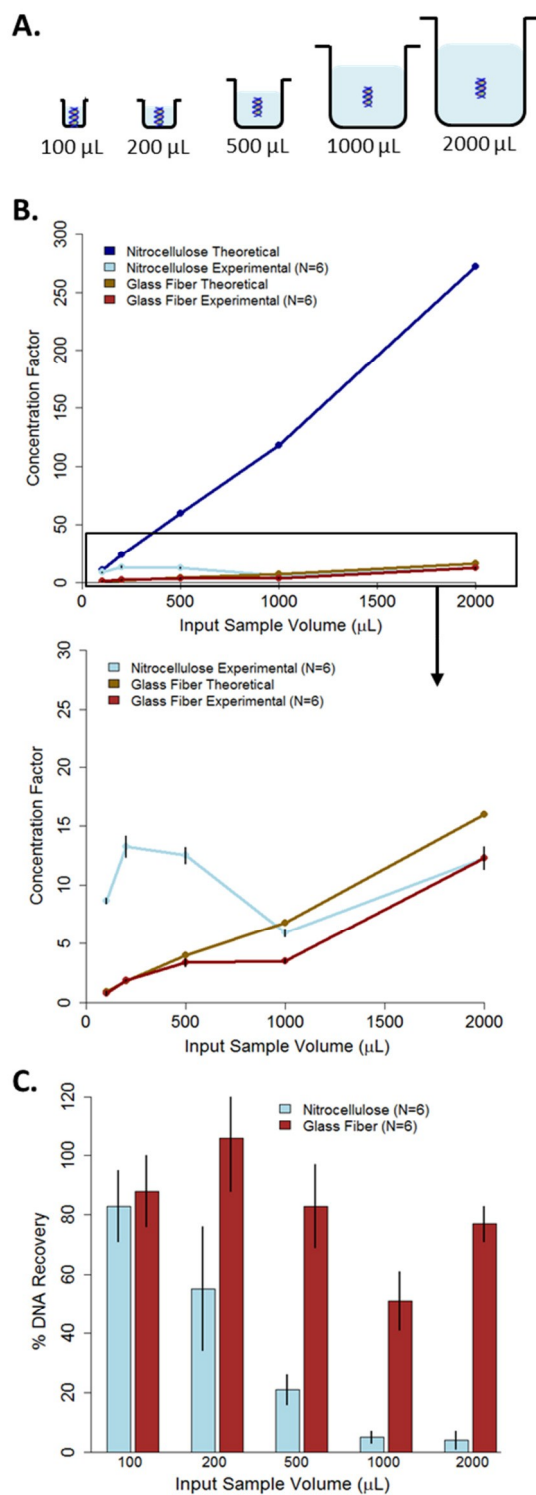
Fig. 4 DNA concentration effects in nitrocellulose and glass fiber. A) Experimental schematic. B) Concentration factor from various input sample volumes. C) Corresponding recovery of DNA from various input sample volumes.

The theoretical concentration factor assumes 100% recovery of DNA. In nitrocellulose, DNA recovery decreased as the

input sample volume increased (**Fig. 4C**), likely due to the time it took to flow large volumes through the membrane. Wicking a 2000 µL sample, followed by 100 µL of wash and elution buffers, through nitrocellulose took over seven hours. This reduced recovery greatly reduced the actual concentration factors achieved in nitrocellulose. The same experiment in glass fiber only took 25 minutes and DNA recovery was independent of input sample volume in (**Fig. 4C**). The long flow times required in nitrocellulose may exceed the chitosan/DNA off-rate which would cause bound DNA to prematurely release from chitosan and be lost to waste. The chitosan-DNA binding constant has been well studied and ranges from 10^9 to 10^{10} M^{-1} [72,73], but, to our knowledge, the chitosan-DNA binding rates have not been published. There have been reported off-rates in the range of $3\text{-}5\times10^{-2}$ s^{-1} [74,75] for similar polycation-DNA interactions.

There are potential applications where concentration factor would matter less than purification but not necessarily recovery. For very dilute samples, such as urine, concentration factor would play a critical role to ensure enough pathogen nucleic acid is recovered for downstream analysis. Additionally, different infections present at a highly variable pathogen loads. For example, clinical studies have quantified active chlamydia infections in urine at 10^1–10^5 elementary bodies/mL[76], ebloa in serum at 10^3–10^9 RNA copies/mL[77], and influenza in nasopharyngeal wash at 10^3–10^7 TCID50/mL[78]. Each of these infections would benefit from a combination of both target purification and concentration. Specifically for infections that occur at low copy number or in dilute samples such as urine, concentration is especially important. Some of these samples would require the processing of larger volumes (mL instead of µL) to ensure a sufficient number of pathogens for infection identification. The current approach, especially using nitrocellulose, is somewhat slow to process larger volumes and may result in decreased recovery (Fig. 4C). The next iteration of this work will involve developing fluidic systems that can rapidly process large volumes in order to purify and concentrate targets from complex, dilute samples.

DNA purification from complex samples
We demonstrated the system's ability to purify DNA from complex sample types. Overall, this method was able to recover ~80% of the input DNA from most of the sample types tested (**Fig. 5**).
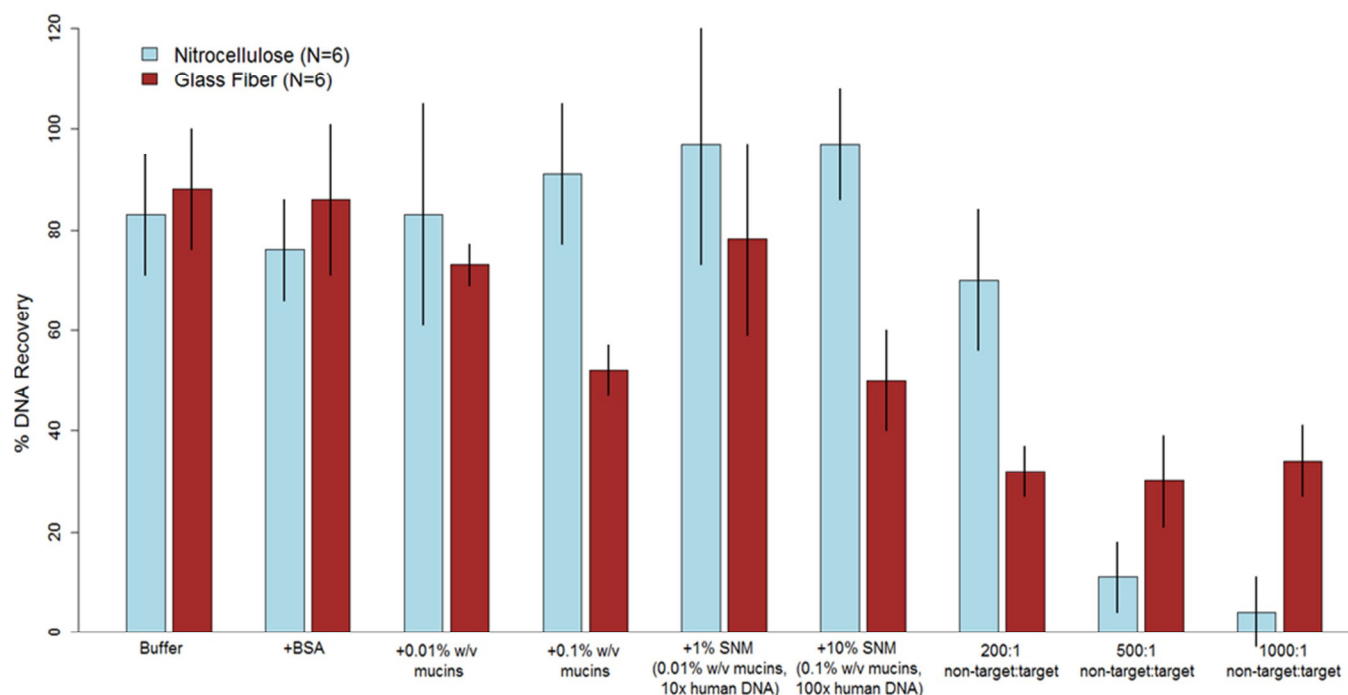
Fig. 5 DNA purification in porous membranes by chitosan capture. Recovery of DNA in either nitrocellulose (blue) or glass fiber (red). The average of N=6 is reported with error bars representing +/- one standard deviation. Chitosan concentration at the capture line was 1.3×10^{-9} µg/µm^2 for nitrocellulose and 1.8×10^{-9} µg/µm^2 for glass fiber. Input DNA was between 1×10^5 and 1×10^6 copies of fragmented MSSA DNA. For SNM: 1% SNM contained 10:1 non-target to target DNA, 0.01% w/v mucins, 1.1 mM NaCl; 10% SNM contained 100:1 non-target to target DNA, 0.1% w/v mucins, 11 mM NaCl.

In both nitrocellulose and glass fiber, the recovery of target DNA was reduced when samples contained a non-target:target ratio of greater than 100:1. These data are slightly higher than the limits dictated by the capacity data above (~10:1 for nitrocellulose and ~20:1 for glass fiber). This discrepancy is likely a result of larger DNA fragments (greater than ~250 kbp)

from the non-target DNA being too large to flow through the small pore features of the membranes. This size-exclusion effect is expected to be more severe in nitrocellulose than in glass fiber due to the differences in pore size distribution between the two membranes. This would suggest that some non-target DNA is essentially filtered upstream of the chitosan capture region rendering it unavailable to compete for binding. The data in Figure 5 support this assumption because at large non-target:target ratios of 200:1, there is a greater reduction in recovery for glass fiber than in nitrocellulose. At higher ratios, 500:1, the reduction in target DNA recovery is similar in both membranes. Recovery of target DNA in glass fiber with an extreme non-target:target ratio of 1000:1 was higher than expected.

The addition of mucins, to mimic nasal swab samples, reduced recovery of target DNA in glass fiber but not in nitrocellulose. Mucins are large protein aggregates (mass>10^6 Da) that are glycosylated with oligosaccharides that commonly form negatively charged side groups[79]. These negatively charged molecules can interact with positively charged chitosan, blocking the binding of DNA. These large aggregates may not pass through the small pores of nitrocellulose because DNA recovery is not affected by their presence in the sample. In glass fiber, however, the larger pores may allow these negatively charged aggregates to flow downstream and prevent DNA binding to chitosan, leading to reduced recovery as the concentration of mucins increases. When both mucins and non-target DNA is present in samples (from simulated nasal matrix, SNM), DNA recovery remains high in nitrocellulose and

decreases in glass fiber. Once again, the magnitude of this decrease is correlated to increasing concentrations of mucins. For applications containing mucins or high concentrations of non-target DNA, the chitosan-patterned region can be extended to increase the system's overall capacity.

DNA purification from blood samples

Blood preparation procedures often require many user steps to remove blood components that can inhibit downstream amplification reactions, notably heme[70]. The chitosan-based DNA purification system is able to rapidly purify target DNA from blood samples with only one user-step (Fig. S7). The eluted samples were quantified by qPCR without further purification.

In both membranes, samples with lower blood concentrations resulted in higher recovery of DNA (**Fig. 6A**). In nitrocellulose, recovery of target DNA from blood-containing samples was significantly inhibited and the flow rate of the sample through the membrane decreased as blood concentration increased. The reduced flow rate appeared to be a result of membrane clogging. For the sample containing 50% blood in nitrocellulose, only a small volume wicked into the membrane before flow stopped completely.

In glass fiber membranes, target DNA was purified from samples containing up to 50% whole blood but, as blood concentration increased, DNA recovery decreased. To verify this result, 50 µL of whole blood plus target DNA was diluted into increasing volumes of buffer. As blood concentration decreased, DNA recovery increased (**Fig. 6B**).
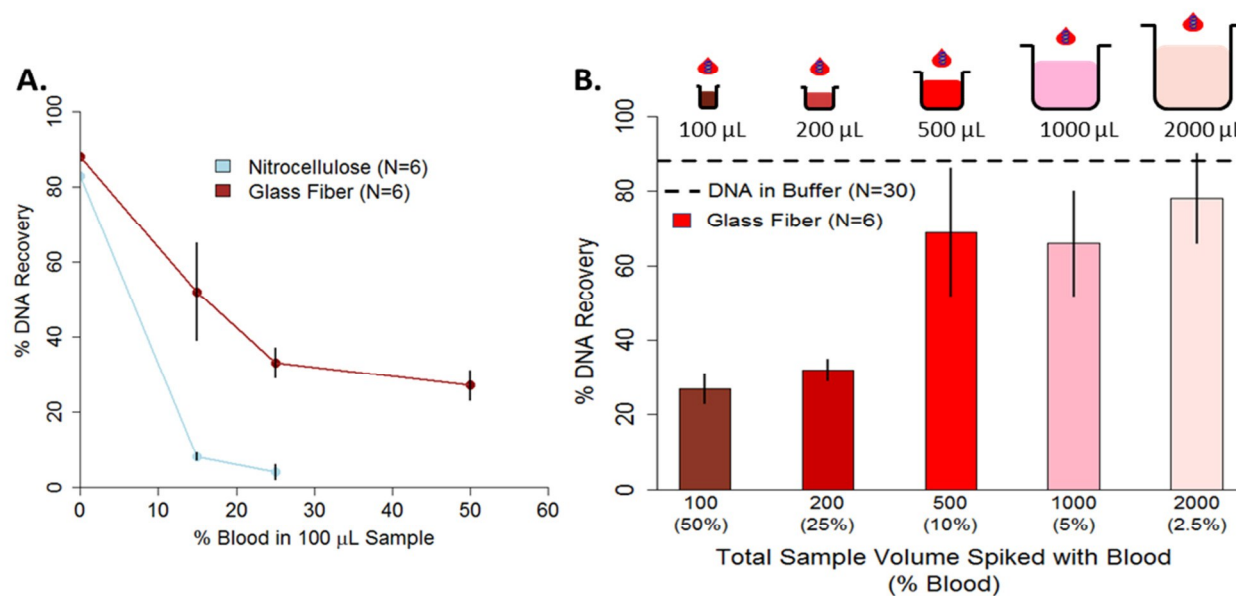
Fig. 6. DNA purification in porous membranes from samples containing blood. The average of N=6 is reported with error bars representing +/- one standard deviation. Chitosan concentration at the capture line was 1.3×10^{-9} µg/µm^2 for nitrocellulose and 1.8×10^{-9} µg/µm^2 for glass fiber. Input DNA was between 1×10^5 and 1×10^6 copies of MSSA DNA. A) Increasing the percent of blood in a 100 µL sample reduced recovery in both nitrocellulose and glass fiber. The 50% blood sample in NC clogged the membrane preventing flow and therefore DNA purification. B) Diluting 50 µL of blood into increasingly large sample volumes improved recovery in glass fiber. For volumes larger than 200 µL, the recovery was similar to the "DNA in buffer" control.

For samples that were less than 25% blood, DNA purification efficiency is similar to the "DNA in buffer" control. This restored recovery is likely due to increased washing of the chitosan region to remove blood components that interfere with chitosan/DNA binding and not with the qPCR analysis. Based on the dilution factor of DNA eluted from chitosan in glass fiber (Fig. S5C) and the sample volume used for qPCR (1 µL of the elution), the maximum amount of blood in a qPCR reaction would be less than 0.5%. For whole blood concentrations at or below 0.5%, qPCR is not inhibited (Fig S3B).

Conclusions

Here we have demonstrated the first example of a system for the simultaneous purification and concentration of DNA from complex samples using chitosan and constructed entirely from porous membranes. First, the interaction of two porous membrane substrates with chitosan was characterized and a method to determine the adsorption capacity of these membranes for polymers was described. Next, to exhibit the broad applicability of this system, it was used to purify DNA from complex samples including those with high protein content, non-target DNA, and known amplification inhibitors such as blood. These samples are just a few examples of potential inputs that can be handled by this system. The choice of membrane provides the ability to control the sample processing time, volume, and concentration factor. Thus, large volume samples such as urine or contaminated environmental water could be rapidly processed with this system at the POC. This method can directly integrate with other paper-based point-of-care technologies such as in-membrane amplification[80] and detection. Further, this system is already well-suited for untrained end users via the use of automatic sequential reagent delivery[63,64]. Future work will therefore demonstrate sample-to-result integrated systems that can rapidly and automatically process high input sample volumes in porous membranes.

Acknowledgements

Notes and References

[a] Address – University of Washington, Department of Bioengineering, 3720 15th Ave NE, Seattle, WA 98195, USA.

* Email: sabyrnes@uw.edu; yagerp@uw.edu

† Electronic Supplementary Information (ESI) available.

1. WHO | Procurement of HIV diagnostics. at <http://www.who.int/diagnostics_laboratory/procurement/hiv/en/>
2. Lozano, R. *et al.* Global and regional mortality from 235 causes of death for 20 age groups in 1990 and 2010: a systematic analysis for the Global Burden of Disease Study 2010. *Lancet* **380,** 2095–128 (2012).
3. Wang, H. *et al.* Age-specific and sex-specific mortality in 187 countries, 1970-2010: a systematic analysis for the Global Burden of Disease Study 2010. *Lancet* **380,** 2071–94 (2012).
4. Murray, C. J. L. *et al.* Disability-adjusted life years (DALYs) for 291 diseases and injuries in 21 regions, 1990-2010: a systematic analysis for the Global Burden of Disease Study 2010. *Lancet* **380,** 2197–223 (2012).
5. Boom, R. *et al.* Rapid and simple method for purification of nucleic acids. *J. Clin. Microbiol.* **28,** 495–503 (1990).
6. Chomczynski, P. Single-Step Method of RNA Isolation by Acid Guanidinium Extraction. *Anal. Biochem.* **159,** 156–159 (1987).
7. Whitesides, G. M. The origins and the future of microfluidics. *Nature* **442,** 368–73 (2006).
8. Price, C. W., Leslie, D. C. & Landers, J. P. Nucleic acid extraction techniques and application to the microchip. *Lab Chip* **9,** 2484–94 (2009).
9. Kim, J., Johnson, M., Hill, P. & Gale, B. K. Microfluidic sample preparation: cell lysis and nucleic acid purification. *Integr. Biol. (Camb.)* **1,** 574–86 (2009).
10. Giordano, B. C., Burgi, D. S., Hart, S. J. & Terray, A. On-line sample pre-concentration in microfluidic devices: a review. *Anal. Chim. Acta* **718,** 11–24 (2012).
11. Bhattacharyya, a & Klapperich, C. M. Design and testing of a disposable microfluidic chemiluminescent immunoassay for disease biomarkers in human serum samples. *Biomed. Microdevices* **9,** 245–51 (2007).
12. Qiu, X. *et al.* Finger-actuated, self-contained immunoassay cassettes. *Biomed. Microdevices* **11,** 1175–86 (2009).
13. Bange, A., Halsall, H. B. & Heineman, W. R. Microfluidic immunosensor systems. *Biosens. Bioelectron.* **20,** 2488–503 (2005).
14. Liu, C., Mauk, M. G. & Bau, H. H. A disposable , integrated loop-mediated isothermal amplification cassette with thermally actuated valves. *Microfluid. Nanofluidics* **11,** 209–220 (2011).
15. White, A. K. *et al.* High-throughput microfluidic single-cell RT-qPCR. *Proc. Natl. Acad. Sci. U. S. A.* **108,** 13999–4004 (2011).
16. Gubala, V., Harris, L. F., Ricco, A. J., Tan, M. X. & Williams, D. E. Point of care diagnostics: status and future. *Anal. Chem.* **84,** 487–515 (2012).
17. Breadmore, M. C. *et al.* Microchip-based purification of DNA from biological samples. *Anal. Chem.* **75,** 1880–6 (2003).
18. Wu, Q. *et al.* Microchip-based macroporous silica sol-gel monolith for efficient isolation of DNA from clinical samples. *Anal. Chem.* **78,** 5704–10 (2006).
19. Tian, H., Hühmer, a F. & Landers, J. P. Evaluation of silica resins for direct and efficient extraction of DNA from complex biological matrices in a miniaturized format. *Anal. Biochem.* **283,** 175–91 (2000).
20. Wen, J., Guillo, C., Ferrance, J. P. & Landers, J. P. DNA extraction using a tetramethyl orthosilicate-grafted photopolymerized monolithic solid phase. *Anal. Chem.* **78,** 1673–81 (2006).
21. Cao, Q. *et al.* Microfluidic chip for molecular amplification of influenza A RNA in human respiratory specimens. *PLoS One* **7,** e33176 (2012).

22. Bhattacharyya, A. & Klapperich, C. M. Thermoplastic microfluidic device for on-chip purification of nucleic acids for disposable diagnostics. *Anal. Chem.* **78,** 788–92 (2006).

23. Cao, Q., Kim, M.-C. & Klapperich, C. M. Plastic Microfluidic Chip for Continuous-Flow Polymerase Chain Reaction: Simulations and Experiments. *Biotechnol. J.* **6,** 177–184 (2012).

24. Chen, D. *et al.* An integrated, self-contained microfluidic cassette for isolation, amplification, and detection of nucleic acids. *Biomed. Microdevices* **12,** 705–19 (2010).

25. Wang, J., Morabito, K., Tang, J. X. & Tripathi, A. Microfluidic platform for isolating nucleic acid targets using sequence specific hybridization. *Biomicrofluidics* **7,** 044107 (2013).

26. Liu, P., Li, X., Greenspoon, S. a, Scherer, J. R. & Mathies, R. a. Integrated DNA purification, PCR, sample cleanup, and capillary electrophoresis microchip for forensic human identification. *Lab Chip* **11,** 1041–8 (2011).

27. Yeung, S. W. & Hsing, I.-M. Manipulation and extraction of genomic DNA from cell lysate by functionalized magnetic particles for lab on a chip applications. *Biosens. Bioelectron.* **21,** 989–97 (2006).

28. Den Dulk, R. C., Schmidt, K. a, Sabatté, G., Liébana, S. & Prins, M. W. J. Magneto-capillary valve for integrated purification and enrichment of nucleic acids and proteins. *Lab Chip* **13,** 106–18 (2013).

29. Liu, X., Erickson, D., Li, D. & Krull, U. J. Cationic polymer coatings for design of electroosmotic flow and control of DNA adsorption. *Anal. Chim. Acta* **507,** 55–62 (2004).

30. Nakagawa, T., Hashimoto, R., Maruyama, K. & Tanaka, T. Capture and Release of DNA Using Aminosilane-Modified Bacterial Magnetic Particles for Automated Detection System of Single Nucleotide Polymorphisms. (2006). doi:10.1002/bit

31. Witek, M. a *et al.* 96-well polycarbonate-based microfluidic titer plate for high-throughput purification of DNA and RNA. *Anal. Chem.* **80,** 3483–91 (2008).

32. Tarmann, C. & Jungbauer, A. Adsorption of plasmid DNA on anion exchange chromatography media. *J. Sep. Sci.* **31,** 2605–2618 (2008).

33. Marshall, L. a, Wu, L. L., Babikian, S., Bachman, M. & Santiago, J. G. Integrated printed circuit board device for cell lysis and nucleic acid extraction. *Anal. Chem.* **84,** 9640–5 (2012).

34. Kenyon, S. M., Meighan, M. M. & Hayes, M. a. Recent developments in electrophoretic separations on microfluidic devices. *Electrophoresis* **32,** 482–93 (2011).

35. Rogacs, A., Marshall, L. a. & Santiago, J. G. Purification of nucleic acids using isotachophoresis. *J. Chromatogr. A* **1335,** 105–120 (2014).

36. Reedy, C. R. *et al.* Dual-domain microchip-based process for volume reduction solid phase extraction of nucleic acids from dilute, large volume biological samples. *Anal. Chem.* **82,** 5669–5678 (2010).

37. Cao, W., Easley, C. J., Ferrance, J. P. & Landers, J. P. Chitosan as a Polymer for pH-Induced DNA Capture in a Totally Aqueous System. *Anal. Chem.* **78,** 7222–7228 (2006).

38. Hagan, K. a, Meier, W. L., Ferrance, J. P. & Landers, J. P. Chitosan-Coated Silica as a Solid Phase for RNA Purification in a Microfluidic Device. *Anal. Chem.* **81,** 8453–8460 (2009).

39. Hagan, K. a *et al.* An integrated, valveless system for microfluidic purification and reverse transcription-PCR amplification of RNA for detection of infectious agents. *Lab Chip* **11,** 957–61 (2011).

40. Danielsen, S., Vårum, K. M. & Stokke, B. T. Structural analysis of chitosan mediated DNA condensation by AFM: influence of chitosan molecular parameters. *Biomacromolecules* **5,** 928–36 (2004).

41. Alatorre-meda, M. *et al.* Colloids and Surfaces B : Biointerfaces The influence of chitosan valence on the complexation and transfection of DNA : The weaker the DNA – chitosan binding the higher the transfection efficiency. *Colloids Surfaces B Biointerfaces* **82,** 54–62 (2011).

42. Prevette, L. E., Kodger, T. E., Reineke, T. M. & Lynch, M. L. Deciphering the role of hydrogen bonding in enhancing pDNA-polycation interactions. *Langmuir* **23,** 9773–84 (2007).

43. Maurstad, G., Danielsen, S. & Stokke, B. T. The influence of charge density of chitosan in the compaction of the polyanions DNA and xanthan. *Biomacromolecules* **8,** 1124–30 (2007).

44. Yagoda, H. Applications of Confined Spot Tests in Analytical Chemistrv. 79–82 (1937).

45. Muller, R. H., Clegg, A. N. D. D. L. & York, N. Automatic Paper Chromatography. 1123–1125

46. Consden, R., Gordon, A. H. & Martin, J. P. Qualitative Analysis of Proteins : a Partition Chromatographic. *Biochem. J.* **38,** 224–232 (1944).

47. Banik, U. K. *et al.* A Simple and Sensitive Nonradioactive Method for the Detection of Urinary Human Chorionic Gonadotropin and Diagnosis of Early Human Pregnancy II Single Unit Test. *Fertil. Steril.* **32,** 426–432 (1979).

48. EPT Do-It-Yourself Early-Pregnancy Test. *Med. Lett. Drugs Ther.* **20,** 30–40 (1978).

49. Arora, S. & Tyagl, S. Detection of Early Pregnancy. *Clinician (Goa).* **42,** 179–183 (1978).

50. Martinez, A. W., Phillips, S. T., Butte, M. J. & Whitesides, G. M. Patterned paper as a platform for inexpensive, low-volume, portable bioassays. *Angew. Chem. Int. Ed. Engl.* **46,** 1318–20 (2007).

51. Fu, E., Lutz, B., Kauffman, P. & Yager, P. Controlled reagent transport in disposable 2D paper networks. *Lab Chip* **10,** 918–20 (2010).

52. Lutz, B. R., Trinh, P., Ball, C., Fu, E. & Yager, P. Two-dimensional paper networks: programmable fluidic disconnects for multi-step processes in shaped paper. *Lab Chip* **11,** 4274–8 (2011).

53. Fridley, G. E., Le, H. Q., Fu, E. & Yager, P. Controlled release of dry reagents in porous media for tunable temporal and spatial distribution upon rehydration. *Lab Chip* **12,** 4321–7 (2012).

54. Fu, E., Kauffman, P., Lutz, B. & Yager, P. Chemical signal amplification in two-dimensional paper networks. *Sens. Actuators. B. Chem.* **149,** 325–328 (2010).

55. Yetisen, A. K., Akram, M. S. & Lowe, C. R. Paper-based microfluidic point-of-care diagnostic devices. *Lab Chip* **13,** 2210–51 (2013).

56. Byrnes, S., Thiessen, G. & Fu, E. Progress in the development of paper-based diagnostics for low-resource point-of-care settings. *Bioanalysis* **5,** 2821–36 (2013).

57. Mariella, R. Sample preparation: the weak link in microfluidics-based biodetection. *Biomed. Microdevices* **10,** 777–84 (2008).

58. Jangam, S. R., Yamada, D. H., McFall, S. M. & Kelso, D. M. Rapid, point-of-care extraction of human immunodeficiency virus type 1 proviral DNA from whole blood for detection by real-time PCR. *J. Clin. Microbiol.* **47,** 2363–8 (2009).

59. Govindarajan, a V, Ramachandran, S., Vigil, G. D., Yager, P. & Böhringer, K. F. A low cost point-of-care viscous sample preparation device for molecular diagnosis in the developing world; an example of microfluidic origami. *Lab Chip* **12,** 174–81 (2012).

60. Linnes, J. C. *et al.* Paper-based molecular diagnostic for Chlamydia trachomatis. *RSC Adv.* **4,** 42245–42251 (2014).

61. Decher, G. Fuzzy Nanoassemblies: Toward Layered Polymeric Multicomposites. *Science (80-.).* **277,** 1232–1237 (1997).

62. Díez-Pascual, A. & Shuttleworth, P. Layer-by-Layer Assembly of Biopolyelectrolytes onto Thermo/pH-Responsive Micro/Nano-Gels. *Materials (Basel).* **7,** 7472–7512 (2014).

63. Bishop, J. *et al.* Sequential Delivery of Fluid Volumes and Associated Devices, Systems and Methods. (2014).

64. Dharmaraja, S. *et al.* Programming paper networks for point of care diagnostics. *Proc. SPIE, 8615, Microfluid. BioMEMS, Med. Microsystems XI* (2013). doi:10.1117/12.2006138

65. Panpradist, N. *et al.* Swab sample transfer for point-of-care diagnostics: characterization of swab types and manual agitation methods. *PLoS One* **9,** e105786 (2014).

66. Eckerskorn, C. & Lottspeich, F. Structural characterization of blotting membranes and the influence of membrane parameters for electroblotting and subsequent amino acid sequence analysis of proteins. 831–838 (1993).

67. Millipore. Rapid Lateral Flow Test Strips.

68. Edelstein, A., Amodaj, N., Hoover, K., Vale, R. & Stuurman, N. Computer control of microscopes using µManager. *Curr. Protoc. Mol. Biol.* **Chapter 14,** Unit14.20 (2010).

69. Abràmoff, M. D., Hospitals, I., Magalhães, P. J. & Abràmoff, M. Image Processing with ImageJ.

70. Akane, a, Matsubara, K., Nakamura, H., Takahashi, S. & Kimura, K. Identification of the heme compound copurified with deoxyribonucleic acid (DNA) from bloodstains, a major inhibitor of polymerase chain reaction (PCR) amplification. *J. Forensic Sci.* **39,** 362–72 (1994).

71. R Core Development Team. R: A language and environment for statistical computing. (2008). at <http://www.r-project.org>

72. Ma, P. L., Lavertu, M., Winnik, F. M. & Buschmann, M. D. New insights into chitosan-DNA interactions using isothermal titration microcalorimetry. *Biomacromolecules* **10,** 1490–9 (2009).

73. Buschmann, M. D. *et al.* Chitosans for delivery of nucleic acids. *Adv. Drug Deliv. Rev.* **65,** 1234–70 (2013).

74. Moriyama, R., Shimada, N., Kano, A. & Maruyama, A. DNA assembly and re-assembly activated by cationic comb-type copolymer. *Biomaterials* **32,** 2351–8 (2011).

75. Wang, Y., Wang, J., Yang, F. & Yang, X. Probing biomolecular interactions with dual polarization interferometry: real-time and label-free coralyne detection by use of homoadenine DNA oligonucleotide. *Anal. Chem.* **84,** 924–30 (2012).

76. Blocker, M. E. *et al.* Quantification of Chlamydia trachomatis Elementary Bodies in Urine by Ligase Chain Reaction. *J. Clin. Microbiol.* **40,** 3631–3634 (2002).

77. Towner, J. S. *et al.* Rapid Diagnosis of Ebola Hemorrhagic Fever by Reverse Transcription-PCR in an Outbreak Setting and Assessment of Patient Viral Load as a Predictor of Outcome Rapid Diagnosis of Ebola Hemorrhagic Fever by Reverse Transcription-PCR in an Outbreak Setting an. *J. Virol.* **78,** 4330–4341 (2004).

78. Wright, P. F., Neumann, G. & Kawaoka, Y. in *Fields Virology* 1692–1740 (1985).

79. Hollingsworth, M. a & Swanson, B. J. Mucins in cancer: protection and control of the cell surface. *Nat. Rev. Cancer* **4,** 45–60 (2004).

80. Rohrman, B. a, Leautaud, V., Molyneux, E. & Richards-Kortum, R. R. A lateral flow assay for quantitative detection of amplified HIV-1 RNA. *PLoS One* **7,** e45611 (2012).